DIRECT-VIEW UNCOOLED MICRO-OPTOMECHANICAL INFRARED CAMERA

M. Mao[1], T. Perazzo[1], O. Kwon, and A. Majumdar[2]
Department of Mechanical Engineering
University of California, Berkeley, CA 94720

J. Varesi and P. Norton
Santa Barbara Research Center (Raytheon)
75 Coromar Drive, Goleta, CA 93117

ABSTRACT

This paper presents the design, fabrication, and the first imaging results of a new uncooled infrared (IR) camera based on thermomechanical sensing and a novel optical readout technique that directly interfaces with the human eye. The system contains a focal plane array (FPA) consisting of bimaterial cantilever beams in each pixel. Absorption of the incident IR radiation by each cantilever beam raises its temperature, resulting in proportional deflection due to mismatch in thermal expansion of the two cantilever materials. A visible optical system is used to simultaneously measure the deflections of all the cantilever beams of the FPA using either Fabry-Perot interferometry or deformable diffraction gratings, and collectively project a visible image of the spatially-varying IR radiation directly on the human eye. The camera is designed to be sensitive in the spectral range of 8-14 μm which is key to night vision. The first results suggest that objects at temperatures as low as 100 °C can be imaged with the best noise-equivalent temperature difference (NEΔT) in the range of 10 K. It is estimated that further improvements that are currently being pursued can improve NEΔT to about 50 mK.

INTRODUCTION

Infrared (IR) vision is a key technology with many applications. Based on measuring the temperature of a distant object, IR vision enables remote sensing, detection and tracking of targets as well as navigation at night and under obscure environments. IR cameras are also used for environmental monitoring of the atmosphere, oceans, and land-based vegetation and mineral resources. The high-cost of IR cameras (>$30K) has, however, restricted their use to few selected applications. If IR cameras were to become inexpensive, i.e., in the range of $1-3 K, a wide range of new commercial applications could be realized. These include night-time navigation for cars, trains and ships, fire detection through walls and through smoke, law enforcement, and night-time oil spill and pollution detection.

For imaging objects near room temperature, IR cameras must absorb radiation in the 8-14 μm range which also happens to be the atmospheric transmission window. Detectors of IR radiation can be broadly classified into two categories - (i) electro-optic, (ii) photothermal. Electro-optic devices have been made with materials such as mercury-cadmium-telluride that have sufficiently small energy bandgaps, ($E_g \approx 0.1$ eV), to detect 8-14 μm IR radiation. However, the small bandgap makes the detector susceptible to thermal noise that varies as $exp\left(-E_g/k_BT\right)$, where T is the temperature and k_B is the Boltzmann constant. The exponential dependence makes cooling to cryogenic temperatures (about 80 K) necessary. The noise-equivalent temperature resolution (NEΔT) for such cryogenic cameras is 5-10 mK. The addition of cooling systems, however, increases weight, cost and poses reliability problems for infrared cameras. This has driven the research towards the development of uncooled detectors which are based on photothermal sensors. The elimination of the cooling system, however, has not reduced the cost over the cryogenic ones, although NEΔT ≈ 20 mK has been achieved. Since the signal from each pixel in all these cameras is electrical, interconnect fabrication to each pixel, scanning electronics, and a visible display system is required in all these cameras. These components all contribute to the high cost of such cameras.

This paper presents a novel design for an IR camera that eliminates many of the high cost components. Figure 1 shows the schematic diagram of the camera, entitled Micro-optomechanical InfraRed Receiver with Optical Readout (MIRROR) system. It contains a focal plane array (FPA) consisting of bimaterial cantilever beams in each pixel. Absorption of the incident IR radiation by each cantilever beam raises its temperature, resulting in proportional deflection due to mismatch in thermal expansion of the two cantilever materials.

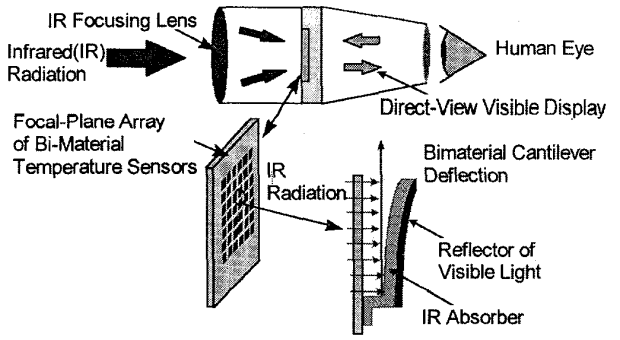

Figure 1: Schematic diagram of micro-optomechanical infrared receiver with optical readout (MIRROR) system.

0-7803-5194-0/99/$10.00 ©1999 IEEE

A visible optical system is used to simultaneously measure the deflections of all the cantilever beams of the FPA and collectively project a visible image of the spatially-varying IR radiation directly on the human eye. The attractive features of the MIRROR system are: (i) uncooled operation is possible since the noise does not exponentially depend on temperature; (ii) direct-view optical readout eliminates the need for electrical interconnects to each pixel, scanning electronics, and an electronic display system, besides reducing fabrication complexity and costs; (iii) in contrast to current uncooled IR cameras, the design of the MIRROR system allows for a low cost, low power, and light weight device.

The use of single bimaterial microcantilevers for temperature and radiation sensing has been demonstrated by several groups [1-6]. Based on this, Manalis et al. [7] made the first attempt to build a camera by fabricating an FPA of Si/Al bimaterial cantilevers which they used to detect absorption of an IR laser operating at 0.78 μm. As will be shown in the next section, Si and Al are not suitable for IR cameras due to their high thermal conductivity as well as lack of absorption in the wavelength range of 8-14 μm. This paper presents the design, fabrication, and the first thermal images using the MIRROR system.

Design of Focal Plane Array

Materials: One of the materials in the cantilever must be an IR absorber in the 8-14 μm and the other must be a good reflector in the visible spectrum. Low-stress silicon nitride (SiN_x) and gold were chosen. Figure 2 shows the real (n) and the imaginary (κ) parts of the refractive index of SiN_x indicating the absorption peak in the 8-14 μm range. Since $\kappa \approx 1$, the penetration depth, $\ell = \lambda/4\pi\kappa$, is about 1 μm in this spectral range. Table 1 provides the properties of SiN_x and Au as well as Si and Al for comparison. SiN_x and Au show the desirable large mismatch in expansion coefficient. In addition, low stress nitride also has low thermal conductivity which is critical for thermal design.

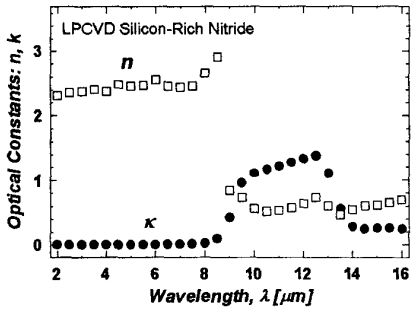

Figure 2: Measurements of the real and the imaginary parts of the refractive index of LPCVD SiN_x.

Table 1: Properties of SiN_x, Au, Si, and Al.

	Density ρ x 10^{-3} kg/m^3	Modulus E, GN/m^2	Thermal Cond., k, W/m-K	Expansion Coeff., α, [x 10^{-6} K^{-1}]	Heat Capacity c, J/kg-K
SiN_x	2.40	180	3	0.8	691
Si	2.33	100	150	2.6	700
Au	19.30	73	296	14.2	129
Al	2.70	80	237	23.6	908

Thermal Design: The temperature rise of a pixel can be expressed as $\Delta T = qA/G$ where q is the absorbed IR flux, A is the cantilever area exposed to IR radiation, and G is the thermal conductance between the cantilever and the surroundings. To maximize ΔT, G must be minimized. The conductance arises from three main contributions, $G = G_{lc} + G_g + G_{rad}$, where G_{lc} is the conductance due to heat conduction through the legs between the pixel and the silicon substrate, G_g is the conductance by the gas, and G_{rad} is the thermal radiative conductance between the pixel and its surroundings. Gas conductance, G_g, can be eliminated by using the FPA in a vacuum. Conductive losses through the leg can be expressed as $G_{lc} = \sum(kwd/L)_i$ where k is the thermal conductivity of the leg material, and w, d, and L are the width, thickness, and length, respectively, of the cantilever leg. To reduce G_{lc}, it is important to use narrow, thin, and long legs made of a low thermal conductivity material. Hence, the leg must not contain any metal or silicon, but should be made of SiN_x or perhaps a material with even lower conductivity. Since the bimaterial cantilever must contain metal, this suggests that the pixels must consist of both metallized and unmetallized regions. The radiative conductance is given as $G_{rad} = 4\sigma(\varepsilon_1 + \varepsilon_2)AT^3$ where σ is the Stefan-Boltzmann constant, and ε_1 and ε_2 are the emissivities of the top and bottom pixel surfaces. Since radiation cannot be eliminated, G_{rad} imposes the lower physical limit of the total conductance. For the 100 μm x 100 μm pixels, $G_{rad} \approx 10^{-8}$ W/K. To reach this limit, the cantilever legs should be designed such that $G_{lc} < G_{rad}$. The thermal time constant of the pixel which quantifies the temporal response of the camera is given as $\tau = C/G$ where $C = \sum(\rho wdLc)_i$ is the thermal capacitance of the pixel. Here ρ is the density and c is the heat capacity. It is desirable to have τ in the range of 10-100 for compatibility with the human eye.

Thermomechanics: To determine the deflection of the cantilever as a function of temperature rise, one must solve the thermomechanical governing equation for a bimaterial cantilever beam, which is given as [5,8]

$$\frac{d^2z}{dx^2} = 6(\alpha_1 - \alpha_2)\left(\frac{d_1 + d_2}{d_2^2 K}\right)\Delta T; \quad z = 0; \frac{dz}{dx} = 0 \text{ at } x = 0 \quad (1)$$

where d is the cantilever thickness, α is the expansion coefficient, z is the cantilever deflection at a distance x. Here $x = 0$ is where the metallization starts and $x = L_m$ is the length of the metallized cantilever. Here, K is a given as

$$K = 4 + 6n + 4n^2 + \phi n^3 + \frac{1}{\phi n}; \quad n = \frac{d_1}{d_2}; \quad \phi = \frac{E_1}{E_2} \quad (2)$$

where E is the elastic moduli, and subscripts 1 and 2 are for the two cantilever materials. Equation (1) can be solved and the sensitivity, $S = \delta/\Delta T$, of the device can be found to be

$$S = \frac{\delta}{\Delta T} = 3(\alpha_1 - \alpha_2)\left(\frac{n+1}{K}\right)\left(\frac{L_m^2}{d_2}\right) \quad (3)$$

where δ is the deflection of the cantilever at $x = L_m$. It is clear from equation (3) that the thermal expansion mismatch must be large. It is also notable that if $n \to 0$ or $n \to \infty$ then $K \to \infty$ and S will be reduced. The optimum value of n depends on

E_1/E_2 which for Au/SiN_x is n_{opt} = 0.8. Equation (3) also indicates that the length must be maximized and the cantilever thickness must be reduced.

IR Optics: Since the IR penetration depth is about 1 μm, the SiN_x thickness was chosen to be 1 μm so that the optical path length for IR radiation in SiN_x became 2 μm due to the presence of the Au reflector on one side. To increase absorption in SiN_x, the gap between the bimaterial cantilever and the silicon substrate was chosen to be 5 μm so that it formed a $\lambda/2$ resonant cavity for 10 μm IR radiation. Figure 3 shows the calculations based on thin film optics [9] for the spectral absorptance of the SiN_x film as a function of film and gap thicknesses.

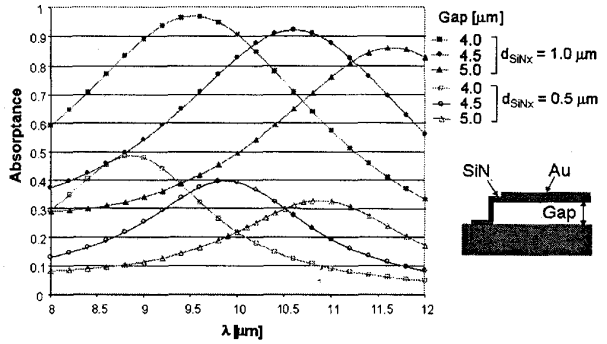

Figure 3: Calculated spectral absorptance of SiN_x film as a function of film and gap thicknesses.

Pixel Tiling: Based on the above design analysis, Fig. 4 shows the pixel design as well as the pixel tiling design that were adopted for the FPA. A staggered tiling of the pixels allowed doubling of the cantilever length (200 μm) for the pixel size (100 μm x 100 μm). Between the anchors and the metallized region of the cantilever were two legs whose lengths totaled 200 μm and provided an estimated thermal conductance, $G_{lc} \approx 10^{-7}$ W/K, which was higher than the radiative limit by a factor of 10. The interdigitated fingers between two adjacent pixels were used as a deformable diffraction grating for optically detecting cantilever deflections (see details later). Note that the fingers on the metallized regions of one pixel meshed with those on the legs of the adjacent pixel. Since the legs were unmetallized and did not deform due to temperature rise, the relative displacement of the diffraction grating was thus maximized.

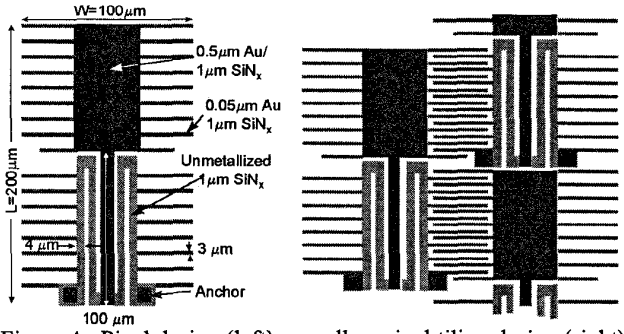

Figure 4: Pixel design (left) as well as pixel tiling design (right) of the FPA.

MICROFABRICATION

The FPAs containing 100 x 100 pixels were fabricated using surface micromachining technology. The process consisted of four masking steps—anchor patterning, thick metal patterning, cantilever definition and thin metal patterning, as shown schematically in Fig. 5.

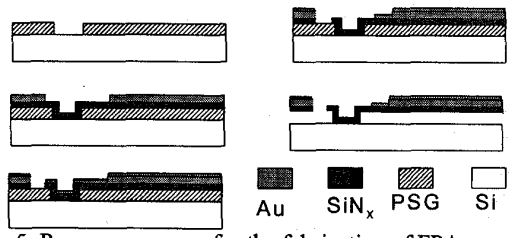

Figure 5: Process sequence for the fabrication of FPA.

The process started with a boron doped silicon wafer with resistivity of 10-20 Ω-cm. The first step was a 5 μm thick LPCVD PSG (phosphorous silicate glass) film deposition and anchor patterning to form the desired gap between the cantilever and the substrate. Second, a 1 μm thick low stress LPCVD silicon nitride film was deposited and followed by thermal evaporation of a 0.5 μm thick gold film on top to form the bimaterial structure. A thin layer of chrome (10 nm) was used to promote the adhesion between the gold and the nitride film. The thick gold film was removed from the regions where the thermal resistance beams and diffraction grating finger structures were formed later. Third, a thin layer of gold (50 nm) was evaporated, and next the cantilever pattern was defined. The fourth step was to remove the unwanted gold layer on the thermal resistance beams. Finally, the PSG sacrificial layer was etched away in HF to release the cantilevers and the FPA was dried using critical point drying to prevent cantilever stiction to the substrate.

Figure 6(a) shows an electron micrograph of typical Au/SiN_x bi-material cantilevers with a length of 200 μm and diffraction grating finger width of 3 μm, as illustrated in Fig. 4. It was observed that the cantilever was slightly bent away from the Si substrate, and the bending at the end of the cantilever measured by the displacement from its original position was about 10 μm at room temperature. This bending was caused by residual stress in the thin films which included the intrinsic stress gradient across the SiN_x and Au films as well as the thermal stress between these two films due to mismatch in expansion coefficients. Figure 6(b) shows the electron micrograph of the cantilevers after all the Au films on top were

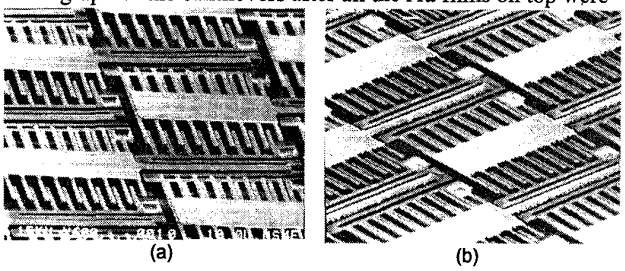

Figure 6: SEM picture of FPA containing bi-material cantilevers (a) partially metallized, (b) bare SiN_x.

removed. It shows that the bare SiN_x cantilevers had intrinsic bending of 4-5 μm at the ends which indicates that the bending caused by metallization was comparable to that of the SiN_x film. Cantilever bending has a major influence on the optical readout system and, hence, its reduction is currently a major research effort.

OPTICAL READOUT

An optical readout is a data acquisition method that measures each pixel's deflection optically as opposed to electronically. The goal of the optical readout is to simultaneously measure deflections of all pixels with sub-nanometer resolution and to display an intensity map based on the collective deflections to our eye or a CCD camera. To clearly define objects in the infrared, the pixel crosstalk should be negligible, i.e. the signal from one pixel should be independent of its neighbor's signal.

Since each cantilever has both a vertical deflection and a slope at its free end there are two basic strategies for measuring cantilever deflection, namely: (i) beam steering based on the slope; and (ii) various vertical deflection methods that will be discussed in detail later. A change in cantilever slope will steer an incident optical beam, thus translating it across a plane. This method is successfully used in the atomic force microscope (AFM) in which a split photodiode, located a few centimeters away from the cantilever, measures the translation of the reflected beam [10]. However, when attempting to measure an array of cantilever deflections, the reflected beams overlap due to diffraction, thus convoluting the signals. The effect of diffraction constrains the measurement plane to be less than 1 mm above the FPA, in which case the required deflection resolution is difficult to achieve by beam-steering methods. Two vertical deflection methods were explored, namely; Fabry-Perot interferometry and a deformable diffraction grating.

Components: The key components in the optical readout are shown in Fig. 7. A small temperature controlled vacuum chamber housed both the FPA and the pinhole array (PHA) chip. To reduce the pixel's gas conductance below the radiation limit a vacuum level of 10 mTorr was required. Since the pixels are sensitive to temperature, all ambient temperature changes must be avoided. Four thermoelectric coolers and a PID controller

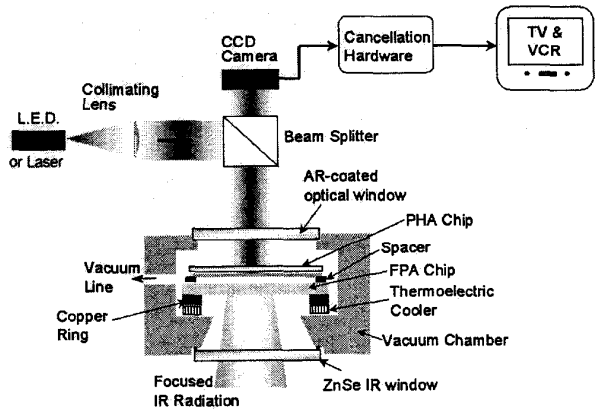

Figure 7: Experimental set up containing optical readout system.

stabilized the temperature to within 0.1°C. A copper ring was used to spread the heat uniformly to the silicon FPA chip. Visible and infrared windows allowed the respective radiation to pass through the vacuum chamber.

Visible light from the HeNe laser was directed to the FPA chip via a non-polarizing beam splitter. The purpose of the CCD camera was to detect this reflected portion of light. The choice of the CCD camera was based on how closely it matched the performance of the human eye. The camera's lens was positioned so that the FPA chip was the viewing plane. Next, the signal from the CCD was processed in real-time to correct non-uniformities in the pixels and visible illumination. Finally, the image was displayed on the TV monitor.

Since the largest vertical deflection occurred at the cantilever's free end, it was advantageous to position the optical beam at this location. The PHA achieved this by masking unwanted light. The PHA was fabricated by depositing a dark mirror coating on a AR coated glass substrate and then patterning the dark mirror coating to leave 30 μm square holes (see Fig. 8) in an array that had a one-to-one correspondence with the pixels in the FPA. At 632 nm the reflectivity and transmissivity of the PHA are less than one percent. The PHA was aligned such that each pixel had a hole directly above it. The FPA and PHA are bonded to each other using adhesive containing glass beads to control their separation (see Fig. 9).

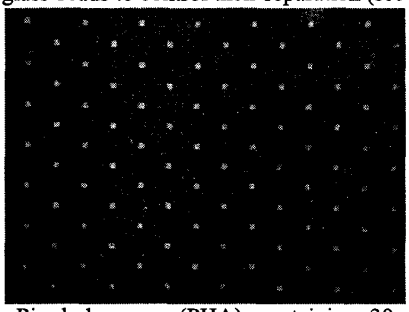

Figure 8: Pin hole array (PHA) containing 30 μm square apertures with one-to-one correspondence with FPA pixels. The remaining region contained a dark mirror coating that had less than 1 percent reflectivity and transmissivity at 632 nm wavelength used in the optical readout system.

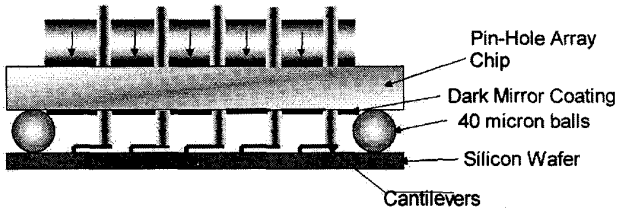

Figure 9: Details of the optical readout system.

Infrared optics are needed to collect the infrared radiation and focus the infrared scene onto the FPA. The collected flux, q α $1/(f/\#)^2$ so a low f/# lens is desirable. The lowest f/# available is around f/0.7. In our experiment an f/1.2 two element lens was used.

Deformable Diffraction Grating: The pixels contained interdigitated fingers that were used as a deformable diffraction

grating as a displacement sensor [11,12]. The fingers attached near the anchor of the pixel deflected less than those located at the free end of the adjacent cantilever. When the PHA was aligned so that the visible light beam was located on the fingers, diffraction occurred depending on the relative distance between fingers. The Helmholtz-Kirchoff integral diffraction theory [13,14] was used to predict the light intensity as a function of finger displacement as shown in Fig. 10.

When the phase difference between fingers is zero, most of the energy is contained in the zeroth order. For a phase difference of 180 degrees, the zeroth order reduces and the first orders contain most of the energy. To exploit this effect, the PHA was located such that all the first order peaks were absorbed in the dark mirror coating and only the zeroth order peak emerged from the PHA (separation distance = 350 μm). The zeroth order went from bright to dark in λ/4 with a gray-scale in between. For incident light at 632 nm and a gray scale of 256 detectable by the human eye and our CCD camera, this corresponded to a vertical resolution of 0.6 nm. The CCD camera monitored the intensity at the PHA which was based on the deflection of a each pixel.

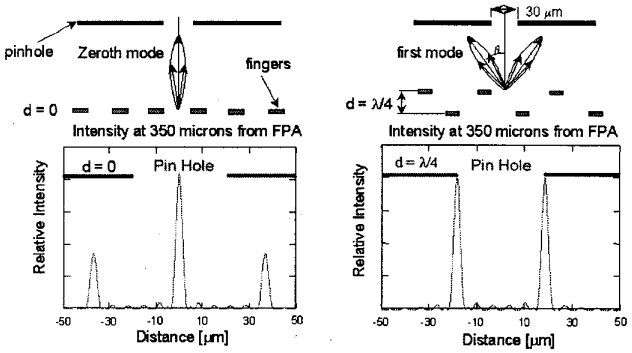

Figure 10: Predictions of Helmholtz-Kirchoff theory for the angular distribution of the diffracted beam at wavelength of 632 nm and for two extreme positions of the deformable diffraction grating. The x-axis in both plots is the location of the spot in the plane of the PHA.

Fabry-Perot Interferometry: The flat metallized region of the pixel between the two rows of interdigitated fingers served as one surface in a Fabry-Perot (F-P) interferometer. The PHA was aligned on the tip of the cantilever. The reference surface needed for interference was the pin hole in the PHA. In this case, the 30 μm apertures in the PHA had a partially reflecting coating. Depending on the phase difference between the two reflected beams the intensity emerging from the pinhole varied from bright to dark. The PHA and the FPA needed to be parallel in this case, since otherwise fringes appeared due to unwanted interference.

IMAGING RESULTS

As a preliminary test, the temperature of the entire FPA was varied to study both optical readout methods. The performance of both methods improved if the initial bending of the cantilevers was zero, thus making it necessary to heat the FPA above room temperature. In our experiments the optimum operating temperature was between 35-85°C which depended on the initial deflection of the cantilevers after fabrication. If the pixel temperature changed 0.1°C or more the intensity of all pixels oscillated until a steady temperature was maintained.

Figure 11 shows infrared images of an electric cooking stove heated to various temperatures, obtained using both optical readout methods. In all F-P interferometry images, vertical dark bands can be seen. We suspect these bands are a result of the angular misalignment of the PHA and the FPA chips. It is extremely difficult with our alignment methods to achieve flatness to within 10 nm required to avoid the observed fringes. This problem was eliminated for the diffraction method since the reference surface for interference was embedded in the adjacent pixels and not on the PHA. Also, in both sets of images there appears to be some pixels that are not as bright as others. This was most likely due to non-uniformities in the pixels.

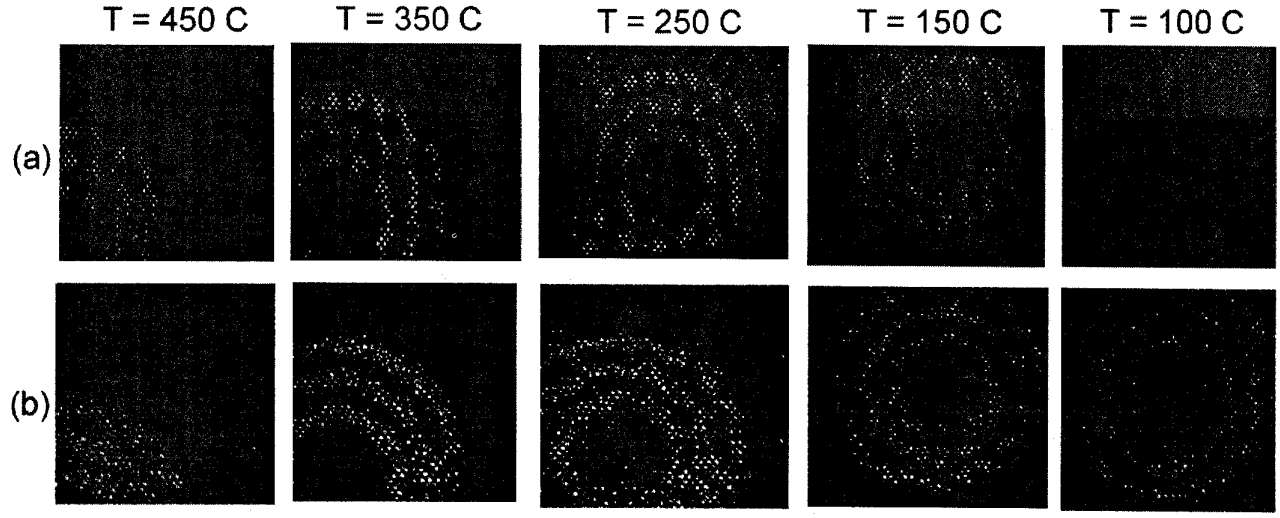

Figure 11: Infrared images of an electric cooking stove at different positions and temperatures, obtained using: (a) Fabry-Perot interferometry; (b) deformable diffraction grating.

The lowest IR source temperature at which infrared images could be observed was about 100 °C. Due to pixel non-uniformity it is difficult to estimate a noise-equivalent temperature difference (NEΔT) for the system. The best pixels exhibited NEΔT in the range of about 10 K for the present design.

Conclusions and Future Directions

This paper presents a new concept of an IR camera based on thermomechanical sensing and an optical readout that interfaces directly with the human eye. Three key technologies are presented here, namely: (i) design of pixels based on materials, thermal, thermomechanical, and IR optical issues; (ii) microfabrication of bimaterial cantilevers with low bending; and (iii) optical readout system that is capable of detecting cantilever deflections with resolution in the 1 nm range and with no pixel cross talk. The first imaging results suggest that objects with temperatures as low as 100 °C can be imaged.

The IR images shown in Fig. 11 represent some of the first ones obtained using the MIRROR system. Although the performance is not bad for the first attempt, it is still far behind the state-of-the-art cameras which have NEΔT of about 10 mK. Hence, the MIRROR system requires much improvement to be commercially viable as an IR camera. A factor of 10 improvement in resolution can be obtained by reducing the leg thermal conductance down to the radiation limit by careful design of the cantilever legs. Note that this is difficult to achieve for pixels with electrical output since the electrical leads are usually made of metal which have higher thermal conductivity than silicon nitride. The IR radiation in the current design has to travel through the Si which does not contain any anti-reflective coating. Hence, the absorptance of the cantilevers is typically about 25 percent of the incident intensity. This can be increased by a factor of 3-4 with proper IR optical design. Finally, with the use of low f/# IR lens, the IR flux can be increased by a factor of 5-6. Putting all these factors together, the temperature resolution can be improved by a factor of about 150-200. This would make the NEΔT in the range of 50 mK. Our theoretical estimate of the best NEΔT is about 5-10 mK, which should make the MIRROR system comparable in performance with other uncooled IR cameras.

Another area which requires significant improvement is microfabrication. The inherent deflections of the tips of cantilevers was about 10 μm at room temperature. It was found that about 50 percent resulted from the bimaterial thermal stress whereas the rest was due to intrinsic stress in the nitride. Our current approach is to design cantilevers where the bimaterial thermal stress and the intrinsic nitride stress cancel each other to produce unbent cantilevers. Finally, emphasis is also being paid towards improving pixel uniformity so that the electronic non-uniformity correction currently used can be eliminated. This would make it truly compatible with the human eye.

Acknowledgments

We are thankful for the support we received from the DARPA MEMS program under contract N66001-97-C-8621, as well as from our program monitors Drs. Elias Towe, Cindy Hanson, and Randy Shimabukuro. We are grateful to Prof. Y. R. Shen of UCB Physics Dept. for sharing several of his lab equipment for our work. M. Ray and R. Anderson from SBRC must be acknowledged for their contributions in some of the microfabrication. Our thanks also to An Huynh of U. of Virginia who helped in the diffraction calculations.

References

[1] J. K. Gimzewski, et al, 'Observation of a chemical reaction using a micromechanical sensor,' *Chem. Phys. Lett., Vol. 217*, '94, pp. 589-594.

[2] J. R. Barnes, et al, 'Photothermal spectroscopy with femtojoule sensitive using a micromechanical device,' *Nature, Vol. 372*, '94, pp. 79-82.

[3] P. I. Oden, et al, 'Uncooled thermal imaging using piezoresistive microcantilever,' *Appl. Phys. Lett., Vol. 69*, '96, pp. 3277-3279.

[4] P. G. Dastkos, et al., 'Remote infrared radiation detection using piezoresistive microcantilevers,' *Appl. Phys. Lett., Vol. 69*, '96, pp. 2986-2988.

[5] J. Lai, et al, 'Optimization and performance of high-resolution micro-optomechanical thermal sensors,' *Sensors and Actuators, Vol. 58*, '97, pp. 113-119.

[6] J. Varesi, et al, 'Photothermal measurements with picoWatt resolution using micro-optomechanical sensors, *Appl. Phys. Lett., Vol. 71*, '97, pp. 306-308.

[7] S. R. Manalis, et al, 'Two-dimensional micromechanical bimorph arrays for detection of thermal radiation,' *Appl. Phys. Lett., Vol. 70,* '97, pp. 3311-3313.

[8] J. R. Barnes, et al, 'A femtojoule calorimeter using micromechanical sensors,' *Rev. Sci. Instrum., Vol. 65*, '94, pp. 3793-3798.

[9] J.A Dobrowolski, *Handbook of Optics,* McGraw-Hill, 1995, pp 42.10-42.14.

[10] D. Sarid, *Scanning Force Microscopy*, Oxford University Press, New York, 1991.

[11] S. Manalis, et al, 'Interdigital cantilevers for atomic force microscopy,' *Appl. Phys. Lett., Vol. 69*, '96, pp. 3944-3946.

[12] G. Yaralioglu, et al, 'Analysis and design of an interdigital cantilever as a dispacement sensor,' *J. Appl. Phys., Vol. 83*, '98, pp. 7405-7415.

[13] J. W. Goodman, *Introduction to fourier optics*, McGraw-Hill, 1968.

[14] M. Born and E. Wolf, *Principles of Optics*, Pergamon Press, 1980.